


Reorientation of antiferromagnetism in cobalt doped FeSn

William R. Meier¹,[✉] Jiaqiang Yan¹,[✉] Michael A. McGuire,¹ Xiaoping Wang^{1,2},
 Andrew D. Christianson,¹ and Brian C. Sales¹

¹Materials Science & Technology Division, Oak Ridge National Laboratory, Oak Ridge, Tennessee 37831, USA

²Neutron Scattering Division, Oak Ridge National Laboratory, Oak Ridge, Tennessee 37831, USA

 (Received 29 July 2019; revised manuscript received 18 October 2019; published 25 November 2019)

FeSn is an itinerant antiferromagnet that hosts electronic Dirac states and ordered magnetic moments lying within its Fe Kagome-lattice planes. We present magnetization measurements of single crystals of $(\text{Fe}_{1-x}\text{Co}_x)\text{Sn}$, revealing the evolution and suppression of this magnetic order with Co substitution. We interpret the dramatic changes in magnetic anisotropy to indicate a reorientation of the moments from perpendicular to parallel to the hexagonal c axis and confirm this with neutron diffraction. It has been proposed that the Dirac nodes observed in FeSn should become gapped if the moments rotate as our data suggests. We identify Co-substituted compositions that adopt both antiferromagnetic configurations at different temperatures. This system provides a unique opportunity to study how the details of magnetic order impact Dirac electron states.

DOI: [10.1103/PhysRevB.100.184421](https://doi.org/10.1103/PhysRevB.100.184421)

I. INTRODUCTION

Topological materials have been a significant focus of the condensed-matter community for the last decade, reviving interest in a number of seemingly simple compounds (e.g. Bi, Bi_2Se_3 , TaAs) [1,2]. Magnetic order has provided another method of tuning the curious electronic states present in these compounds [3–5]. FeSn is an excellent example of a compound where electronic degeneracy may be tuned with magnetic order [6,7].

FeSn adopts a B35 hexagonal structure ($P6/mmm$, No. 191) composed of Sn-filled Fe-Kagome layers (see inset of Fig. 1) separated by sheets of Sn [8,9]. FeSn is an itinerant antiferromagnet below $T_N = 365$ K [9–16]. This phase is characterized by nearly collinear Fe-moments \perp [001] within the Kagome layers which are aligned antiparallel to their neighboring layers along the c axis [8,11–13] (sketched in left inset of Fig. 1).

Dirac nodes have been identified in the electronic structure in FeSn [6,7]. This is significant because this electronic degeneracy is present in its magnetically ordered state. Lin *et al.* [6] proposed that the Dirac nodes at the H -point in FeSn become gapped if the antiferromagnetic moments were rotated to an axial orientation.

CoSn is isostructural with FeSn [9,17] but does not order magnetically [15]. These compounds do form a complete solid solution, $(\text{Fe}_{1-x}\text{Co}_x)\text{Sn}$, with evolving magnetic properties investigated in Ref. [9] above room temperature.

In this paper, we investigate the systematic evolution of the anisotropic magnetic properties of $(\text{Fe}_{1-x}\text{Co}_x)\text{Sn}$ single crystals below 380 K. The results suggest a cobalt substitution induces a reorientation of ordered magnetic moments from the antiferromagnetic arrangement in FeSn and ultimate suppression of magnetic order (summarized in Fig. 1). The dramatic temperature variation of magnetization suggests that the antiferromagnetic moments rotate continuously from a planar to an axial orientation via an intermediate tilted phase producing a pair of sharp features. We confirm this moment rotation

with neutron diffraction. Based on the prediction in Ref. [6], we propose an illustrative angular resolved photoemission experiment to observe the gapping-out and re-establishment of the Dirac nodes in a single $(\text{Fe}_{0.94}\text{Co}_{0.06})\text{Sn}$ sample. This composition exhibits all three antiferromagnetic phases (axial, tilted, and planar) below the Néel temperature.

II. METHODS

Crystals of $(\text{Fe}_{1-x}\text{Co}_x)\text{Sn}$ were grown by flux growth from a melt of 98 or 97 at. % tin in alumina crucibles by cooling

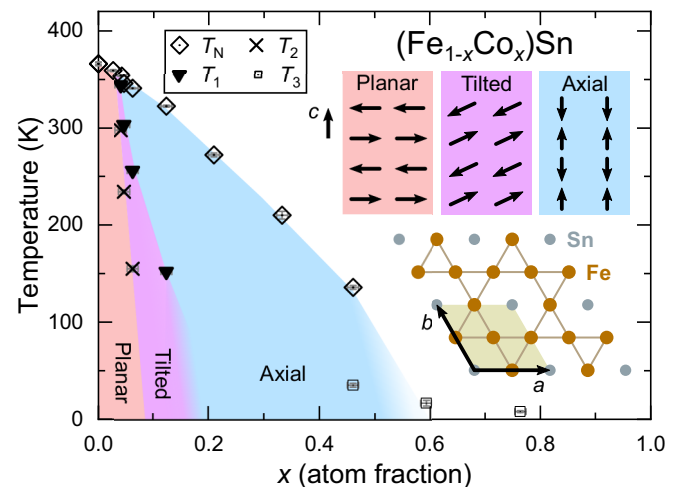


FIG. 1. Magnetic phase diagram of $(\text{Fe}_{1-x}\text{Co}_x)\text{Sn}$ showing suppression and reorientation of antiferromagnetism with Co substitution. The planar magnetic order observed in FeSn remains the ground state for $x < 0.09$. Right of the transition delineated by T_2 samples adopt a tilted phase with moments rotating smoothly from an in-plane orientation before locking into the axial phase at the transition T_1 . The top insets depict the transition-metal moments of the proposed magnetic phases. The bottom inset shows a projection of the FeSn crystal structure.

from 800 to 600 °C over 200 h. See Appendix A for details of the growth and resulting crystals.

These crystals were characterized by powder x-ray diffraction (PANalytical X'pert Pro, with Cu-K α radiation). The refined lattice parameters are presented in Appendix B and confirm a complete solid solution between FeSn and CoSn as reported in Ref. [9]. Chemical compositions were determined with a Bruker Quantax 70 energy dispersive spectrometer on polished crystals in a Hitachi TM3000 scanning electron microscope. These compositions are used throughout this paper.

Magnetization measurements were performed on single crystals in a Quantum Design Magnetic Property Measurement System (MPMS) from 2–380 K in plastic drinking straws. An applied field of 1 kOe was chosen as it was generally below a change in slope observed in some magnetization vs field data [10,18]. Four-probe electrical resistivity was measured on crystals shaped into bars contacted with Pt wire and Ag epoxy (H20E) giving contact resistances of 1–4 Ω . Samples were measured between 2 and 390 K with the ac-transport option of a 9 T Quantum Design Physical Property Measurement System (PPMS). Heat capacity measurements were carried out in the same PPMS using the Quantum Design heat capacity option. Apiezon N-grease was used between 1.8 and 300 K using dense addenda steps (2.5 K) above 190 K to mitigate the effects of grease characteristics in this temperature range [19,20]. Apiezon H-grease was used to measure heat capacity from 200 to 380 K.

Neutron diffraction was carried out on a 3.6-mg single crystal of $(\text{Fe}_{0.94}\text{Co}_{0.06})\text{Sn}$ with the TOPAZ single-crystal diffractometer at the Spallation Neutron Source [21,22]. Sample temperature was controlled by a nitrogen cryostream and the time-of-flight data from the 25 spherically arranged detectors was processed with Mantid [23]. All plots presented were generated with the same crystal orientation.

III. RESULTS

First, we will discuss the physical properties of an illustrative dilute-Co sample compared to undoped FeSn. The top panel of Fig. 2 presents the anisotropic magnetization versus temperature data. The Néel transition in FeSn is evident as a maximum in the magnetization. Cooling below this, the signal remains nearly constant (≈ 0.036 emu/g) along [001] but is suppressed in-plane. This magnetic anisotropy ($M_{\parallel}/M_{\perp} \approx 1.3$ as $T \rightarrow 0$ K) arises from the relative ease of the planar Fe-moments (oriented \perp [001]) [8,11–13] to cant to follow a field along [001] [24].

The magnetic behavior of the cobalt-substituted crystal (brown curves) is strikingly complicated, producing cliff and inverted shark-fin shaped magnetization curves. Again, both orientations display a maximum in magnetization signaling the onset of antiferromagnetism at 340 K but the anisotropy is reversed just below. Unlike pure FeSn, the susceptibility \perp [001] retains the larger, constant value while the response along [001] drops dramatically on cooling until $T_1 = 255$ K (minimum $M_{\parallel}/M_{\perp} = 0.4$). This can be explained by the development of axial ordered-moments (\parallel [001]) which respond more to an applied field in the ab plane than along [001]. The magnetization of isostructural FeGe shows simi-

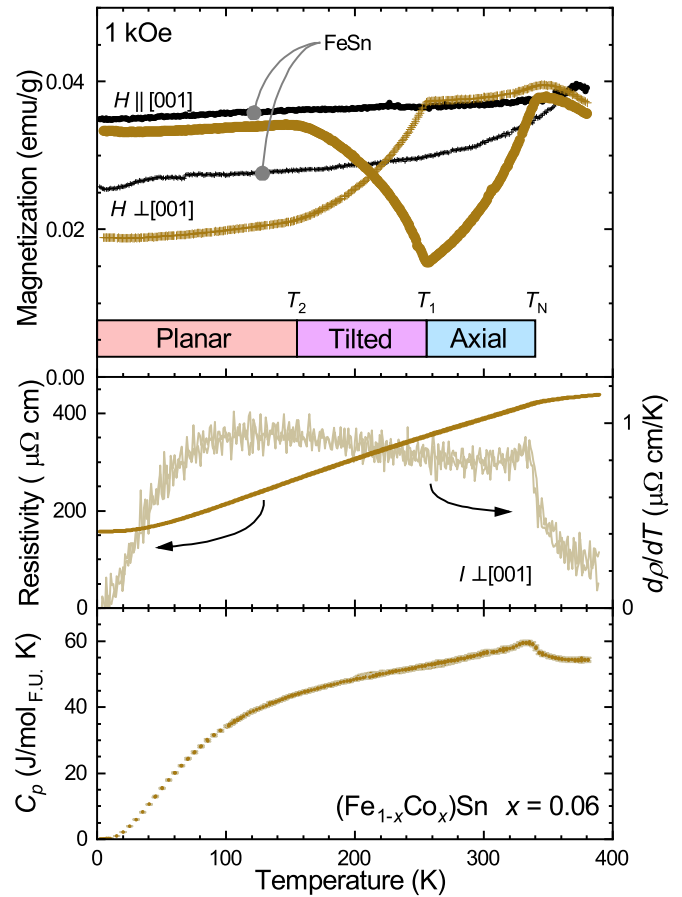


FIG. 2. Magnetization, resistivity and heat capacity versus temperature of $(\text{Fe}_{0.96}\text{Co}_{0.06})\text{Sn}$ (brown curves). Magnetization versus temperature (top) shows dramatic variations in magnetic anisotropy compared to FeSn (thinner, black curves). Sharp features at $T_1 = 255$ K and $T_2 = 155$ K signal transitions between antiferromagnetic orders with distinct orientation of magnetic moments labeled with colored bars. Resistivity (ρ , middle) and heat capacity (bottom) do not present discernible features at T_1 or T_2 .

lar anisotropic response [25–27] and has been demonstrated to adopt this axial antiferromagnetic order between 55 and 410 K [28–30].

This anisotropy is dramatically and continuously reversed between T_1 and $T_2 = 155$ K, below which the response is relatively constant ($M_{\parallel}/M_{\perp} = 1.8$). Note that the values of magnetization along [001] and sign of anisotropy of both samples are comparable at low temperatures, suggesting a similar planar antiferromagnetic order. Finally, the magnetization curves of $(\text{Fe}_{0.96}\text{Co}_{0.06})\text{Sn}$ are continuous through both T_1 and T_2 implying second-order transitions [31]. The curious progression of magnetic response of Co-doped FeSn with temperature clearly signal changes in its magnetic order.

Resistivity measurements on a crystal of $(\text{Fe}_{0.94}\text{Co}_{0.06})\text{Sn}$ from the same batch (middle of Fig. 2) reflect little of the changes evident in magnetization data. The sample shows metallic behavior between 2 and 390 K with $R(300\text{ K})/R(2\text{ K}) = 2.5$ with $I \perp$ [001]. This resistance ratio is dramatically lower than pure FeSn (≈ 154) [10]. This is primarily a consequence of a substantially larger residual

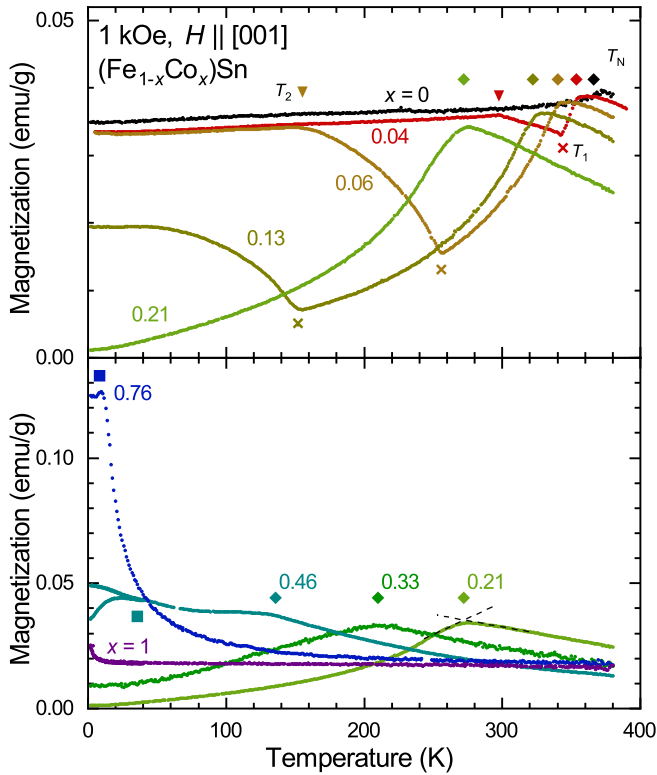


FIG. 3. Evolution of axial magnetization of $(\text{Fe}_{1-x}\text{Co}_x)\text{Sn}$ single crystals. Transitions of each curve are highlighted by matching colored symbols: T_N diamonds, T_1 \times 's, T_2 triangles, and T_3 squares. Transitions were defined by the intercept of extrapolations of the curve on either side as shown for $x = 0.21$. Samples with $x \geq 0.46$ display a deviation of field-cooled and zero-field-cooled magnetization marked with a square as exemplified by $x = 0.46$ below 35 K.

resistance ($\text{FeSn} \approx 1.6$ and $\text{Co-doped} \approx 158 \mu\Omega\text{cm}$ for $I \perp [001]$) likely due to disorder on the transition metal site. There is a clear kink in the resistance curve corresponding to $T_N = 340$ K. Plotting the derivative emphasizes this feature but neither resistance or its derivative show any feature corresponding to T_1 and T_2 . This suggests that these changes in magnetism have little impact on the electronic scattering and structure (near the Fermi energy).

The heat-capacity measurements of $(\text{Fe}_{0.94}\text{Co}_{0.06})\text{Sn}$ at the bottom of Fig. 2 also show frustratingly little sensitivity to the events at T_1 and T_2 . We clearly observe a second-order jump in C_p at T_N similar to that observed in FeSn [10]. There are no discernible jumps in the $C_p(T)$ curve at T_1 or T_2 , suggesting very little entropy is associated with these transitions.

Now we turn to the striking variation of this magnetic behavior across the FeSn-CoSn series. The systematic evolution of $H \parallel [001]$ magnetization curves are presented in Fig. 3 for selected compositions. First, consider the monotonic suppression of T_N (indicated by diamonds) with increasing cobalt up to $x = 0.46$. When cooled below this temperature crystals with $x > 0.03$ show a steep drop in c -axis susceptibility in contrast to pure FeSn ($x = 0$). Once again, we propose that this signals an antiferromagnetic phase with axial moments developing immediately below T_N .

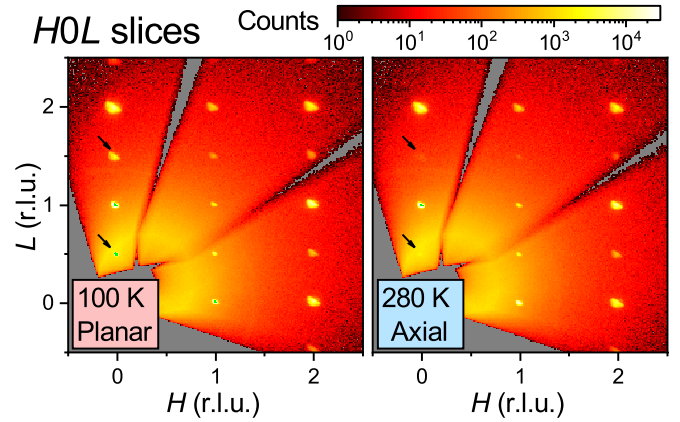


FIG. 4. Neutron diffraction data from a $(\text{Fe}_{0.94}\text{Co}_{0.06})\text{Sn}$ crystal. Slices of the $H0L$ plane are presented at 100 and 280 K, revealing peak intensities at half-integer L consistent with the planar and axial moment configurations, respectively. Indices are based on the paramagnetic unit cell. Bins with more than 30 000 counts are green.

As observed with $x = 0.06$, the magnetization trend reverses sharply on cooling through T_1 (marked with \times 's). The c -axis magnetization increases until it reaches the magnitude of the $x = 0$ curve and abruptly levels off for $x = 0.04$ and 0.06 at T_2 (marked with triangles). We interpret this as the tilted phase with a continuous evolution of moment orientations from the axial ($\parallel [001]$) to the planar phase identified in undoped FeSn on cooling. The magnetization of $x = 0.13$ never attains the magnetization of the lower- x samples below T_1 . In our model, this indicates that the moments never lock into a purely planar orientation in this sample.

The data from the three highest- x samples display a divergent behavior to a low temperature maximum on cooling (marked with squares). This is discussed in Appendix C and we focus here on the changes in antiferromagnetism at lower-Co concentrations.

Finally, neutron diffraction data from a crystal with $x = 0.06$ at 100 and 280 K are presented in Fig. 4 (additional temperatures in Appendix D). In both cases, magnetic Bragg peaks at half-integer L signal commensurate antiferromagnetic order with a propagation vector $(00\frac{1}{2})$ (r.l.u. in the paramagnetic cell). Critically, the peaks at $(00\frac{1}{2})$ and $(00\frac{3}{2})$ (indicated with arrows) are significantly weaker (500 and 20 times, respectively) at 280 K than 100 K. We infer that the ordered moments are parallel to $[001]$ at 280 K based on these nearly absent peaks. This confirms our picture of ordered moments developed from the magnetization data.

IV. DISCUSSION

We interpret the graceful evolution of magnetization curves presented in Fig. 3 to signal a reorientation of antiferromagnetic moments from planar to axial as presented in Fig. 1. These two phases have been identified in FeSn [11] and FeGe [26,28–30], respectively. Between $x \approx 0.03$ to 0.2 , samples pass through an intermediate (tilted) phase where the moment orientations smoothly rotate between the two orientations.

In this picture, the transitions at T_1 and T_2 correspond to the unlocking/locking of moments to the axial and planar orientations.

Neutron diffraction results reveal the antiferromagnetic propagation vector is $(00\frac{1}{2})$ in the planar, tilted, and axial phases. This indicates moments simply rotate while retaining the same ferromagnetic in-plane and antiferromagnetic out-of-plane correlations in all three phases.

Next, we want to address the weak intensity at $(00\frac{1}{2})$ and $(00\frac{3}{2})$ in the 280 K plot of Fig. 4. If the moments are aligned along $[001]$, as we assert, there should not be elastic peaks with these scattering vectors. One explanation for this unexpected intensity is inelastic scattering by low-energy, transverse magnons because TOPAZ doesn't have energy discrimination for elastic scattering. We suspect that the static moments are completely axial between 255 and 340 K based on the magnetization data in Fig. 2.

We rationalize the absence of distinct features in resistance versus temperature at T_1 and T_2 in Fig. 2 by remembering the itinerant character of antiferromagnetism in this system. The changes in the electronic structure that occur at T_N appear to have a limited effect on resistivity, producing only a subtle kink. Reorientation of the ordered moments is expected to modify the crossing of specific electronic bands well below the Fermi energy [6]. This would have little impact on the terms that determine electrical resistivity [32]. In addition, these subtle band modifications do not release significant entropy, explaining the absence of features in the heat capacity data below T_N . Resistance or heat-capacity features are absent at a similar moment reorientation identified in YbFe_6Ge_6 [33].

The reorientation we propose has important implications for the electronic bands. The planar antiferromagnetic state of FeSn has been shown to host Dirac fermion features in its electronic structure [6,7]. Lin *et al.* go on to note that these nodes should gap out if the moment orientation is axial (as they are no longer protected crystallographic symmetry) [6].

This is exactly the situation we believe is present in $(\text{Fe}_{1-x}\text{Co}_x)\text{Sn}$. In fact, compositions near $x = 0.06$ provide exciting samples for study as they appear to pass through all three phases on cooling; axial (gapped nodes), tilted (gapped?), and planar (ungapped). We propose that angular-resolved photoemission experiments could observe the gapping of the Dirac nodes in the axial phase. After cooling further, this gap should reclose as the moments adopt the planar configuration below T_2 .

This system can also provide insights into controlling and understanding magnetic anisotropy in itinerant systems. This has an important implication for discovery and engineering of ferromagnets [34,35] and the understanding of antiferromagnetism in other correlated systems [36,37].

Finally, Fig. 1 depicts how T_N is suppressed by Co substitution, trending to 0 K somewhere near $x = 0.6$. Tuning a phase transition to 0 K is a common theme in condensed-matter physics [38,39]. Along these lines, new features are observed in magnetization data for composition in the neighborhood of $x \approx 0.6$ below 40 K discussed briefly in Appendix C. We plan to investigate this carefully in the future to understand what is happening in this regime.

V. CONCLUSIONS

We examined the curious evolution of magnetic properties of $(\text{Fe}_{1-x}\text{Co}_x)\text{Sn}$ single crystals. Based on our results, we determine that the magnetic moments reorient from the planar orientation, identified in FeSn, to axial with cobalt substitution. These phases are separated by a tilted phase where the moments smoothly rotate between the two configurations. The planar antiferromagnetic state in FeSn has been demonstrated to host Dirac nodes which are proposed to gap-out if the moments align along the c axis. We propose that a sample that adopts each phase at different temperatures (e.g., $x = 0.06$) is an ideal candidate for a photoemission experiment to test for gapped and ungapped nodes in each case.

ACKNOWLEDGMENTS

We would like to thank A. May and S. Okamoto for their helpful discussions. Research was supported by the U.S. Department of Energy, Office of Science, Basic Energy Sciences, Materials Sciences and Engineering Division under Contract No. DE-AC05-00OR22725. This research used resources at the Spallation Neutron Source, a DOE Office of Science User Facility operated by Oak Ridge National Laboratory.

This paper has been co-authored by employees of UT-Battelle, LLC under Contract No. DE-AC05-00OR22725 with the U.S. Department of Energy. The U.S. Government retains and the publisher, by accepting the paper for publication, acknowledges that the U.S. Government retains a nonexclusive, paid-up, irrevocable, worldwide license to publish or reproduce the published form of this paper, or allow others to do so, for U.S. Government purposes. The Department of Energy will provide public access to these results of federally sponsored research in accordance with the DOE Public Access Plan [40].

APPENDIX A: CRYSTAL GROWTH

Sn shot (Alfa Aesar Puratronics, 99.9999% metals basis), Fe granules (Alfa Aesar, 99.98% metals basis), and Co

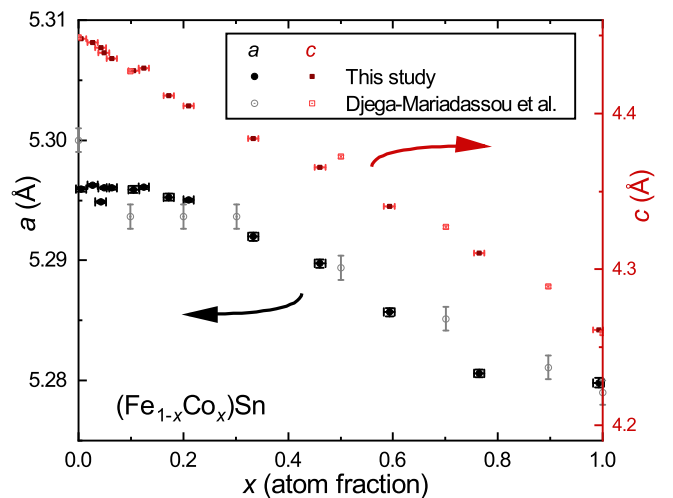


FIG. 5. Hexagonal lattice parameters of $(\text{Fe}_{1-x}\text{Co}_x)\text{Sn}$ as a function of composition determined by energy dispersive spectroscopy. Reported data from Djega-Mariadassou *et al.* [9] are plotted for comparison.

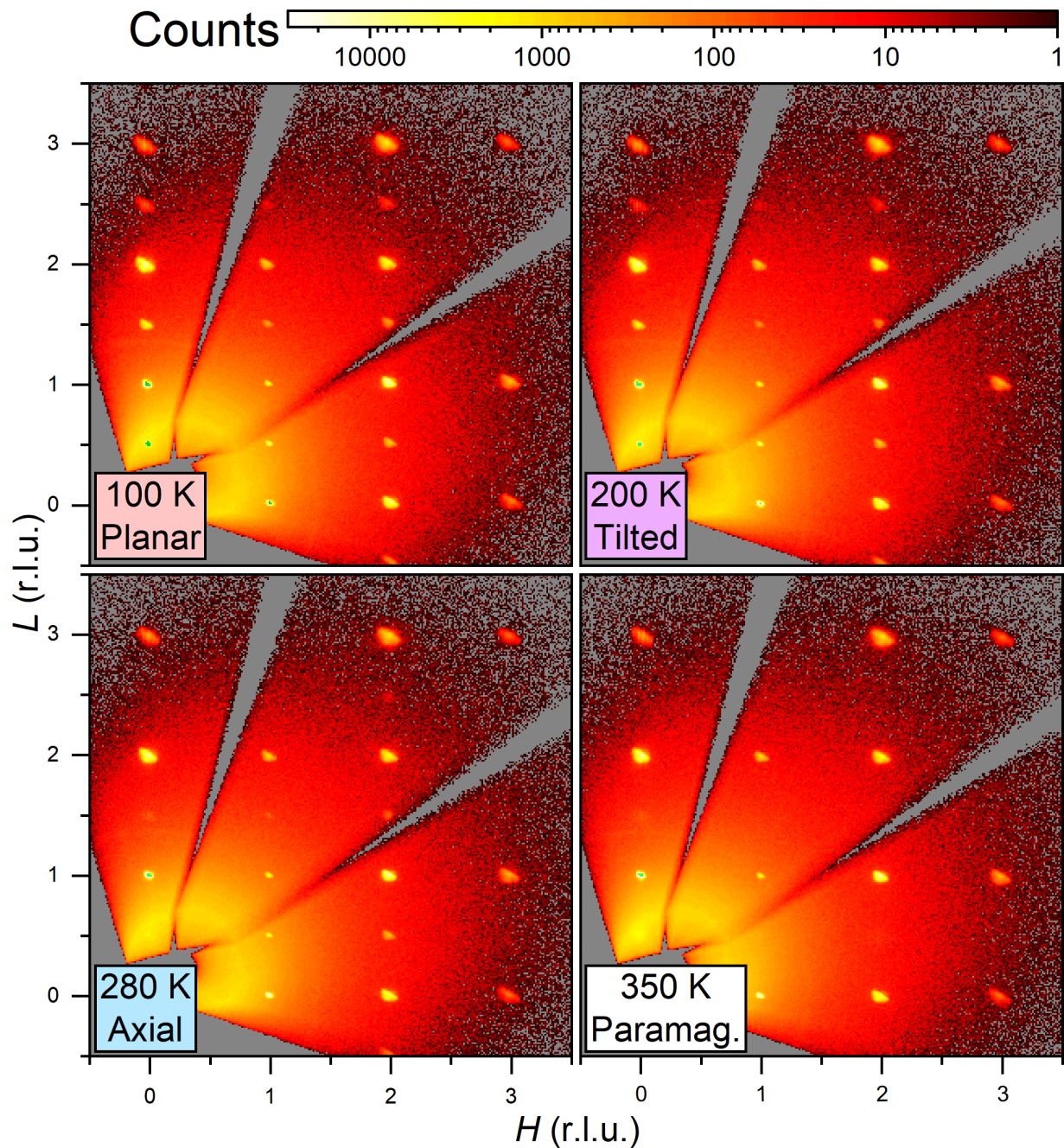


FIG. 6. Neutron diffraction results from a single crystal of $(\text{Fe}_{0.94}\text{Co}_{0.06})\text{Sn}$ collected with the TOPAZ instrument. HOL slices of the diffraction data are presented for temperatures in each of the phases identified in this sample. The crystal orientation and exposure are the same for all. The upper scale was adjusted to emphasize antiferromagnetic peaks and bins with more than 30 000 counts are colored green.

powder (Alfa Aesar, 99.998% metals basis) totaling 6.5 g were loaded into a 2 mL Canfield Crucible Set [41]. This was sealed in a fused-silica ampoule under vacuum.

This ampoule assembly was heated in a box furnace to 1100°C over 9 h then held for 12 h to pull the transition metals into solution. Next the furnace was cooled to 1000°C in 3 h and held for 48 h. During this time, the furnace was opened and each ampoule was shaken to stir the melt [10,42]. Next the furnace was cooled to 800°C over 28 h then slowly cooled to 600°C over 200 h to grow the crystals. Finally, the ampoule was removed from the furnace and inverted into a centrifuge

to rapidly fling off liquid Sn. The properties of FeSn can vary with quench temperature [10], therefore we emphasize that all samples were quenched from 600°C by this centrifuge procedure.

The crystals obtained by this procedure ranged from 0.5 to 2 mm stubby, hexagonal rods and plates for Fe-rich compositions to 0.05 by 6 mm hexagonal needles at the Co-rich end. All crystals exhibited bright, metallic facets and were brittle with cleavage along (001). The mass of $(\text{Fe}_{1-x}\text{Co}_x)\text{Sn}$ crystals obtained decreased with Co additions as the solubility of Co in Sn is higher than Fe [43–45]. This is why we used

98 and 97 at. % Sn for Fe and Co rich batches, respectively. Residual Sn on the surface of crystals could be removed by soaking in a 37% HCl solution for 1-3 h. This procedure had to be watched carefully because the (001) facets of the $(\text{Fe}_{1-x}\text{Co}_x)\text{Sn}$ crystals were etched noticeably and blackened while the other facets remained shiny.

APPENDIX B: LATTICE PARAMETERS

Figure 5 shows that lattice parameters of the FeSn-CoSn solid solution series determined by powder x-ray diffraction. The lattice shrinks in both the a and c directions with Co additions in agreement with the Djega-Mariadassou *et al.* [9].

APPENDIX C: LOW-TEMPERATURE PHASE

A low-temperature peak is observed in the magnetization versus temperature for crystals with higher cobalt concentrations (Fig. 3). This behavior is clearly distinct from T_N in the $x = 0.46$ sample. In $x = 0.46, 0.59$ (not shown), and 0.76 the maximum is associated with a divergence (marked with squares) in the field-cooled and zero-field cooled magnetization curves (shown only for $x = 0.46$).

Potential explanations for this low-temperature magnetic response include impurities, spin glass behavior or a new magnetic phase. Spin-glass behavior or another magnetic ground state are possibilities as either could be the result of the suppression of antiferromagnetic order toward a quantum

critical point with Co-doping. Determining the origin of this magnetic response is a short-term goal.

APPENDIX D: NEUTRON DIFFRACTION

Neutron-diffraction results from a single crystal of $(\text{Fe}_{0.94}\text{Co}_{0.06})\text{Sn}$ are presented as HOL slices in Fig. 6 at four key temperatures. Peaks are indexed with respect to the paramagnetic FeSn unit cell. In the paramagnetic state (350 K), only nuclear Bragg peaks appear with integer H and L . On cooling through $T_N = 340$ K, magnetic peaks appear with half-integer L in the 280 K plot. This signals the development of antiferromagnetic order with propagation vector $00\frac{1}{2}$ r.l.u. and a doubling of the hexagonal unit-cell along the c axis. The peaks on the $00L$ line are very weak compared to $(10\frac{1}{2})$ because of the orientation of the magnetic moments in the axial phase. At 200 K, the antiferromagnetic, half-integer L peaks on the $00L$ line are significantly stronger as moment component perpendicular to $[001]$ develops in the tilted phase. Finally, at 100 K strong intensity is observed at all low- Q antiferromagnetic peaks.

Initially, one might expect the fully planar moments we propose at 100 K to create reduced intensity peaks with scattering vectors nearly perpendicular to $(00L)$. There are at least three orientations for domains for the planar antiferromagnet. Strong intensity is still observed at $(20\frac{1}{2})$ because this scattering vector has a component perpendicular to the ordered moments in some of these domains.

-
- [1] M. Z. Hasan and C. L. Kane, Colloquium: Topological insulators, *Rev. Mod. Phys.* **82**, 3045 (2010).
- [2] N. P. Armitage, E. J. Mele, and A. Vishwanath, Weyl and Dirac semimetals in three-dimensional solids, *Rev. Mod. Phys.* **90**, 015001 (2018).
- [3] C.-Z. Chang, J. Zhang, X. Feng, J. Shen, Z. Zhang, M. Guo, K. Li, Y. Ou, P. Wei, L.-L. Wang, Z.-Q. Ji, Y. Feng, S. Ji, X. Chen, J. Jia, X. Dai, Z. Fang, S.-C. Zhang, K. He, Y. Wang, L. Lu, X.-C. Ma, and Q.-K. Xue, Experimental observation of the quantum anomalous Hall effect in a magnetic topological insulator, *Science* **340**, 167 (2013).
- [4] R. S. K. Mong, A. M. Essin, and J. E. Moore, Antiferromagnetic topological insulators, *Phys. Rev. B* **81**, 245209 (2010).
- [5] M. Hirschberger, S. Kushwaha, Z. Wang, Q. Gibson, S. Liang, C. A. Belvin, B. A. Bernevig, R. J. Cava, and N. P. Ong, The chiral anomaly and thermopower of Weyl fermions in the half-Heusler GdPtBi, *Nat. Mater.* **15**, 1161 (2016).
- [6] Z. Lin, C. Wang, P. Wang, S. Yi, L. Li, Q. Zhang, Y. Wang, Z. Wang, Y. Sun, Z. Sun, J.-H. Cho, C. Zeng, and Z. Zhang, Dirac fermions in antiferromagnetic FeSn Kagome lattices with combined space inversion and time reversal symmetry, [arXiv:1906.05755v1](https://arxiv.org/abs/1906.05755v1) (2019).
- [7] M. Kang, L. Ye, S. Fang, J.-S. You, A. Levitan, M. Han, J. I. Facio, C. Jozwiak, A. Bostwick, E. Rotenberg, M. K. Chan, R. D. McDonald, D. Graf, K. Kaznatcheev, E. Vescovo, D. C. Bell, E. Kaxiras, J. van den Brink, M. Richter, M. P. Ghimire, J. G. Checkelsky, and R. Comin, Dirac fermions and flat bands in the ideal kagome metal FeSn, [arXiv:1906.02167v1](https://arxiv.org/abs/1906.02167v1) (2019).
- [8] L. Häggström, T. Ericsson, R. Wäppling, and K. Chandra, Studies of the magnetic structure of FeSn using the Mössbauer effect, *Phys. Scr.* **11**, 47 (1975).
- [9] C. Djega-Mariadassou, P. Lecocq, and A. Michel, Étude magnétique et structurale des phases $M\text{Sn}_2$ et $M\text{Sn}$ ($M = \text{Fe}, \text{Co}$) et des solutions solides $(\text{Fe}_x\text{M}_{1-x})\text{Sn}$, $(\text{Fe}_x\text{M}_{1-x})\text{Sn}_2$ ($M = \text{Co}, \text{Ni}$), *Ann. Chimie* **4**, 175 (1969).
- [10] B. C. Sales, J. Yan, W. R. Meier, A. D. Christianson, S. Okamoto, and M. A. McGuire, Quasi 2-D magnetism in the Kagome layer compound FeSn, [arXiv:1907.07719](https://arxiv.org/abs/1907.07719) [Phys. Rev. Materials (to be published)].
- [11] K. Yamaguchi and H. Watanabe, Neutron diffraction study of FeSn, *J. Phys. Soc. Jpn.* **22**, 1210 (1967).
- [12] S. Ligenza, A spin-flip effect in FeSn, *Phys. Status Solidi (b)* **45**, 721 (1971).
- [13] S. Ligenza, A Mössbauer study of hyperfine parameters of Sn119 in antiferromagnetic and paramagnetic states of FeSn, *Phys. Status Solidi (b)* **50**, 379 (1972).
- [14] H. Yamamoto, Mössbauer effect measurement of intermetallic compounds in iron-tin system: Fe_5Sn_3 and FeSn, *J. Phys. Soc. Jpn.* **21**, 1058 (1966).
- [15] L. Häggström, T. Ericsson, R. Wäppling, E. Karlsson, and K. Chandra, Mössbauer studies of the isostructural compounds FeGe, FeSn and CoSn, *J. Phys. Colloques* **35**, C6-603 (1974).
- [16] R. Masrour, E. K. Hlil, M. Hamedoun, A. Benyoussef, O. Mounkachi, and H. E. Moussaoui, Electronic and magnetic structures of FeSn compound investigated by first principle, mean field and series expansions calculations, *Physica A: Stat. Mech. Appl.* **414**, 249 (2014).

- [17] A. S. Mikhaylushkin, T. Sato, S. Carlson, S. I. Simak, and U. Häussermann, High-pressure structural behavior of large-void CoSn-type intermetallics: Experiments and first-principles calculations, *Phys. Rev. B* **77**, 014102 (2008).
- [18] M. Kakihana, K. Nishimura, D. Aoki, A. Nakamura, M. Nakashima, Y. Amako, T. Takeuchi, T. Kida, T. Tahara, M. Hagiwara, H. Harima, M. Hedo, T. Nakama, and Y. Ōnuki, Electronic states of antiferromagnet FeSn and Pauli paramagnet CoSn, *J. Phys. Soc. Jpn.* **88**, 014705 (2019).
- [19] W. Schnelle, J. Engelhardt, and E. Gmelin, Specific heat capacity of Apiezon N high vacuum grease and of Duran borosilicate glass, *Cryogenics* **39**, 271 (1999).
- [20] Quantum Design, Non-smooth specific heat between 200 K and 300 K due to anomalous specific heat of Apiezon N-grease, 2014.
- [21] A. J. Schultz, M. R. V. Jørgensen, X. Wang, R. L. Mikkelsen, D. J. Mikkelsen, V. E. Lynch, P. F. Peterson, M. L. Green, and C. M. Hoffmann, Integration of neutron time-of-flight single-crystal Bragg peaks in reciprocal space, *J. Appl. Crystallogr.* **47**, 915 (2014).
- [22] G. Jogl, X. Wang, S. A. Mason, A. Kovalevsky, M. Mustyakimov, Z. Fisher, C. Hoffman, C. Kratky, and P. Langan, High-resolution neutron crystallographic studies of the hydration of the coenzyme cob(II)alamin, *Acta Crystallogr. Sec. D Biol. Crystallogr.* **67**, 584 (2011).
- [23] O. Arnold, J. C. Bilheux, J. M. Borreguero, A. Buts, S. I. Campbell, L. Chapon, M. Doucet, N. Draper, R. F. Leal, M. A. Gigg, V. E. Lynch, A. Markvardsen, D. J. Mikkelsen, R. L. Mikkelsen, R. Miller, K. Palmen, P. Parker, G. Passos, T. G. Perring, P. F. Peterson *et al.*, Manti-data analysis and visualization package for neutron scattering and SR experiments, *Nucl. Instr. Meth. Phys. Res. Sec. A: Accel., Spectrometers, Detectors Assoc. Equipment* **764**, 156 (2014).
- [24] S. Blundell, *Magnetism in Condensed Matter* (Oxford University Press, Oxford, UK, 2001).
- [25] O. Beckman, K. Carrander, L. Lundgren, and M. Richardson, Susceptibility measurements and magnetic ordering of hexagonal FeGe, *Phys. Scr.* **6**, 151 (1972).
- [26] J. Bernhard, B. Lebech, and O. Beckman, Neutron diffraction studies of the low-temperature magnetic structure of hexagonal FeGe, *J. Phys. F: Metal Phys.* **14**, 2379 (1984).
- [27] O. Beckman, L. J. Sundström, K. Carrander, and L. Lundgren, Localized versus itinerant electrons in hexagonal FeGe, *Solid State Commun.* **12**, 1061 (1973).
- [28] J. Bernhard, B. Lebech, and O. Beckman, Magnetic phase diagram of hexagonal FeGe determined by neutron diffraction, *J. Phys. F* **18**, 539 (1988).
- [29] J. B. Forsyth, C. Wilkinson, and P. Gardner, The low-temperature magnetic structure of hexagonal FeGe, *J. Phys. F* **8**, 2195 (1978).
- [30] L. Häggström, T. Ericsson, R. Wäppling, and E. Karlsson, Mössbauer study of hexagonal FeGe, *Phys. Scr.* **11**, 55 (1975).
- [31] *Phase Transformations in Materials*, edited by G. Kostroz (Wiley-VCH, Weinheim, Germany, 2001).
- [32] C. Kittel, *Introduction to Solid State Physics* (John Wiley & Sons Inc, Hoboken, NJ, 2004).
- [33] M. A. Avila, T. Takabatake, Y. Takahashi, S. L. Bud'ko, and P. C. Canfield, Direct observation of Fe spin reorientation in single-crystalline YbFe₆Ge₆, *J. Phys.: Condens. Matter* **17**, 6969 (2005).
- [34] M. A. McGuire, K. V. Shanavas, M. S. Kesler, and D. S. Parker, Tuning magnetocrystalline anisotropy by cobalt alloying in hexagonal Fe₃Ge, *Sci. Rep.* **8**, 14206 (2018).
- [35] B. C. Sales, B. Saparov, M. A. McGuire, D. J. Singh, and D. S. Parker, Ferromagnetism of Fe₃Sn and alloys, *Sci. Rep.* **4**, 7024 (2014).
- [36] W. Lv and P. Phillips, Orbital and magnetically induced anisotropy in iron-based superconductors, *Phys. Rev. B* **84**, 174512 (2011).
- [37] M. Hoyer, R. M. Fernandes, A. Levchenko, and J. Schmalian, Disorder-promoted C₄-symmetric magnetic order in iron-based superconductors, *Phys. Rev. B* **93**, 144414 (2016).
- [38] P. Coleman and A. J. Schofield, Quantum criticality, *Nature* **433**, 226 (2005).
- [39] P. C. Canfield and S. L. Bud'ko, Preserved entropy and fragile magnetism, *Rep. Prog. Phys.* **79**, 084506 (2016).
- [40] <http://energy.gov/downloads/doe-public-access-plan>.
- [41] P. C. Canfield, T. Kong, U. S. Kaluarachchi, and N. H. Jo, Use of frit-disc crucibles for routine and exploratory solution growth of single crystalline samples, *Philos. Mag.* **96**, 84 (2016).
- [42] H. J. Scheel and E. O. Schulz-Dubois, Flux growth of large crystals by accelerated crucible-rotation technique, *J. Crystal Growth* **8**, 304 (1971).
- [43] H. Giefers and M. Nicol, High pressure x-ray diffraction study of all Fe–Sn intermetallic compounds and one Fe–Sn solid solution, *J. Alloys Compd.* **422**, 132 (2006).
- [44] H. Okamoto, *Binary Alloy Phase Diagrams*, 2nd ed. (ASM International, Materials Park, OH, 1990), Chap. Fe–Sn (Iron–Tin), p. 1774.
- [45] H. Cömert and J. N. Pratt, Constitutional studies of cobalt-tin alloys, *Metall. Trans. A* **23**, 2401 (1992).